NANO LETTERS

pubs.acs.org/NanoLett Letter

Abnormal Out-of-Plane Vibrational Raman Mode in Electrochemically Intercalated Multilayer MoS_2

Yufei Sun, Shujia Yin, Ruixuan Peng, Jia Liang, Xin Cong, Yi Li, Chenyu Li, Bolun Wang, Miao-Ling Lin, Ping-Heng Tan,* Chunlei Wan,* and Kai Liu*

Cite This: *Nano Lett.* 2023, 23, 5342−5349 Read Online

ACCESS | Metrics & More | Article Recommendations | Supporting Information

ABSTRACT: Raman spectroscopy is a powerful technique to probe structural and doping behaviors of two-dimensional (2D) materials. In MoS_2, the always coexisting in-plane (E^1_{2g}) and out-of-plane (A_{1g}) vibrational modes are used as reliable fingerprints to distinguish the number of layers, strains, and doping levels. In this work, however, we report an abnormal Raman behavior, i.e., the absence of the A_{1g} mode in cetyltrimethylammonium bromide (CTAB)-intercalated MoS_2 superlattice. This unusual behavior is quite different from the softening of the A_{1g} mode induced by surface engineering or electric-field gating. Interestingly, under a strong laser illumination, heating, or mechanical indentation, an A_{1g} peak gradually appears, accompanied by the migration of intercalated CTA^+ cations. The abnormal Raman behavior is mainly attributed to the constraint of the out-of-plane vibration due to intercalations and resulting severe electron doping. Our work renews the understanding of Raman spectra of 2D semiconducting materials and sheds light on developing next-generation devices with tunable structures.

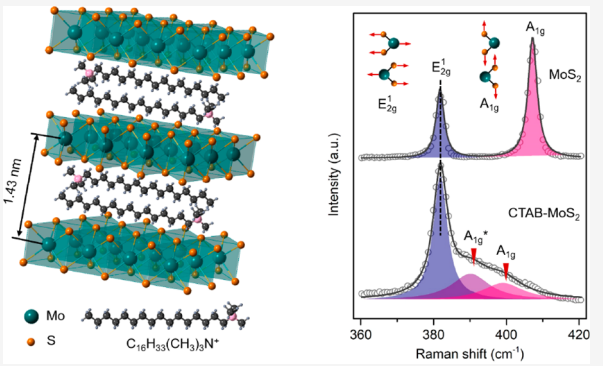

KEYWORDS: *CTAB-MoS_2, Raman behavior, electron doping, interlayer coupling*

Two-dimensional (2D) layered materials emerge as promising candidates for the next-generation electronics because of their unique structures and extraordinary properties.[1−3] Delicate characterizations of 2D materials are of vital importance for the studies of their structures and functions. Raman spectroscopy is one of the most widely used characterization methodologies because of its fast speed and nondestructive detection.[4,5] Phonon Raman scattering originates from the lattice vibration of materials and can be regarded as the fingerprint of a material, which is capable of probing the lattice structures, layer numbers, functional groups, doping, interlayer coupling, and strain condition of 2D materials.[6−9] The study of Raman behaviors will further deepen the understanding in the phonons, electron−phonon, and electron−electron interactions of 2D materials, which will be helpful in both fundamental science and industrial applications.

As a typical transition-metal dichalcogenide (TMDC), MoS_2 has attracted growing attention in the past decade. Semiconducting 2H-MoS_2 has shown great potential as an atomically thick key material in electronic devices, optical and optoelectronic devices, and catalysis.[10−12] The Raman spectra of 2H-MoS_2 yield two characteristic peaks, namely E^1_{2g} and A_{1g}, in the range of 360−440 cm^{-1}, corresponding to the Mo−S in-plane vibration and out-of-plane vibrations, respectively.[13−15] The positions of these two Raman peaks are widely used to analyze the strain condition, doping, and interlayer coupling in MoS_2.[5,6,16,17] In particular, the peak interval between E^1_{2g} and A_{1g} peaks is an indicator of the number of layers of MoS_2 flakes. For simplicity, we still use the irreducible representations E^1_{2g} and A_{1g} of bulk 2H-MoS_2 for few-layer MoS_2, although they should belong to different irreducible representations in odd- and even-layer MoS_2 due to the different point group symmetries.[5] Usually, when the peak interval is less than 20 cm^{-1}, the MoS_2 flake is a monolayer, while the peak interval of 20−22 cm^{-1} corresponds to a bilayer MoS_2 and the interval of more than 23 cm^{-1} to a tri- or multilayer MoS_2.[6,13] Further studies reveal that the E^1_{2g} mode is susceptible to in-plane strain and the A_{1g} mode is more sensitive to doping,[16,18] resulting in the fact that monolayer MoS_2 possibly exhibits peak interval of more than 20 cm^{-1} on certain substrates or in specific environments. In spite of the deviations in peak interval, the E^1_{2g} and A_{1g} Raman modes are regarded as the most apparent fingerprint of MoS_2, which always coexist regardless of substrates or environments.

Received: April 25, 2023
Revised: May 17, 2023
Published: May 23, 2023

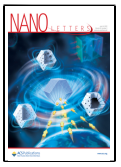

https://doi.org/10.1021/acs.nanolett.3c01543
Nano Lett. 2023, 23, 5342−5349

In this work, however, we found that there is only a single evident E^1_{2g} Raman mode in electrochemically intercalated MoS_2 (CTAB-MoS_2), where the A_{1g} Raman mode disappears (or is highly suppressed). This abnormal Raman behavior is quite different from the softening of the out-of-plane A_{1g} vibration by some treatments.[18,19] It is found that with increasing the laser power the E^1_{2g} mode remains almost unchanged in peak position, but the A_{1g} peak gradually becomes visible and blue-shifts by several cm^{-1} until it reaches the position like that in a "normal" MoS_2.[13,14] The renormalization process can also be achieved by heating the sample or indenting its surface with a large mechanical pressure and is found to accompany the migration of the intercalated cetyltrimethylammonium cations (CTA^+), suggesting that the interface interaction between the MoS_2 and CTA^+ plays a vital role in the abnormal Raman behavior. We attribute the abnormal Raman behavior to the constraint of the out-of-plane vibration induced by the intercalations and the electron-doping effect induced by the electrochemical intercalation process. Such a strong and consistent electron-doping effect can hardly be achieved by other approaches such as surface engineering or electric-field gating, which opens a new pathway for enhancing the electron density of layered 2D semiconducting materials.

CTAB-intercalated MoS_2 crystals (Figure 1a) were synthesized by electrochemical intercalation of bulk MoS_2 as described in previous work (see Figure S1 and Methods section for details).[20] The cathode reaction can be described as $xCTA^+ + MoS_2 + xe^- = (CTA^+)_xMoS_2^{x-}$.[21] X-ray diffraction (XRD) analysis shows that the (002) peak of pure bulk MoS_2 locates at $2\theta = 14.31°$, corresponding to an interlayer distance of $d(MoS_2) = 0.62$ nm (Figure 1b). As a comparison, the (002) peak of CTAB-MoS_2 (inset of Figure 1b) shifts to $2\theta = 6.17°$, which yields an interlayer distance of d(CTAB-MoS_2) = 1.43 nm. Cross-sectional HRTEM was also used to clarify the structure of CTAB-MoS_2, revealing a hexagonal structure with the (100) lattice plane spacing of 0.27 nm, similar to that of pristine MoS_2, while the interlayer distance is 1.40 nm, consistent with the XRD analysis (Figure S2). As the diameter of an individual CTA^+ chain is 0.46−0.51 nm,[22] it is estimated that double-layer CTA^+ chains antiparallelly stack into the van der Waals (vdWs) gap of MoS_2,[21] as shown in Figure 1a.

The abnormal Raman spectra were observed under a 532 nm excitation wavelength in thin CTAB-MoS_2 flakes mechanically exfoliated from a bulk crystal (Figure 1c). As shown in Figures 1d and S3, the E^1_{2g} mode of the sample peaks at ~381 cm^{-1} with relatively high intensities like those of pure MoS_2 samples.[13] However, the A_{1g} peak exhibits an abnormal behavior; i.e., it appears to vanish while a new broad Raman mode emerges nearby the E^1_{2g} peak. This abnormal behavior exists in many CTAB-MoS_2 samples, but for some other ones the behavior is not so evident where the A_{1g} peaks are only red-shifted from its normal position (around 408 cm^{-1}).[5] For all of the CTAB-MoS_2 samples, we found it more accurate to analyze their Raman spectra with a multipeak fitting, namely, E^1_{2g}, A_{1g}*, and A_{1g}. Here, the peak ranging from 395 to 410 cm^{-1} is ascribed to the A_{1g} peak, while the peak ranging from 385 to 395 cm^{-1} is called the A_{1g}* peak, which reflects the abnormal Raman behavior of CTAB-MoS_2 samples and was not reported in the literature. The assignment of A_{1g}* peak is determined by its polarized behavior and temperature-dependent behavior in Raman spectra, which will be further discussed below. The

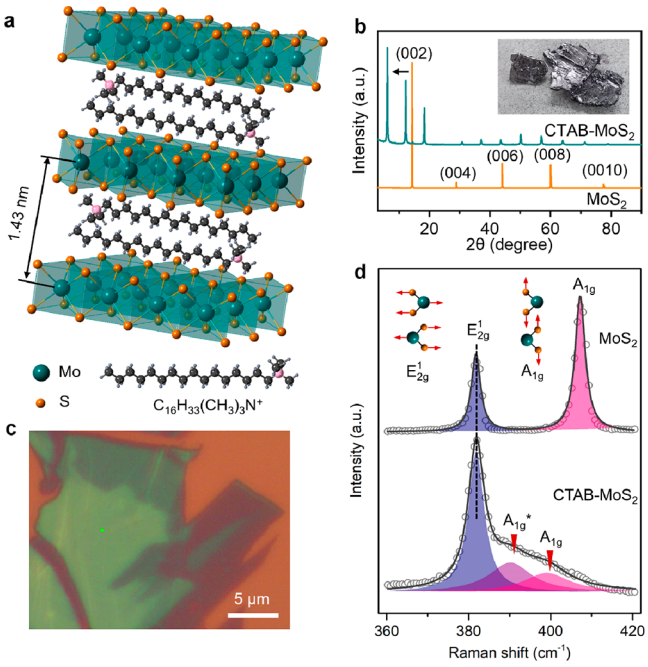

Figure 1. Crystal structure and Raman characterization of CTAB-MoS_2 superlattices. (a) Crystal structure of CTAB-MoS_2, with double-layer CTA^+ antiparallelly stacked between MoS_2 layers. (b) XRD analysis of bulk natural MoS_2 (orange line) and CTAB-MoS_2 (cyan line). All peaks of MoS_2 originate from (002) plane family and indexed. All peaks of CTAB-MoS_2 are also from (002) plane family but have shifted to lower degree, indicating an enlarged interlayer distance. Inset shows the optical photo of the bulk CTAB-MoS_2. (c) Optical microscopy image of a CTAB-MoS_2 thin flake exfoliated on Si/SiO_2 substrate. (d) Raman spectra of CTAB-MoS_2 (lower) and pure MoS_2 (upper) flakes. In comparison with pure MoS_2, the A_{1g} peak of CTAB-MoS_2 is severely suppressed and red-shifted, and there exists a broad peak near the E^1_{2g} peak, namely A_{1g}*. Inset shows the vibrational mode of E^1_{2g} and A_{1g}.

A_{1g}* and A_{1g} can also be observed under 488 and 633 nm laser excitations (Figure S4).

The abnormal Raman behavior of CTAB-MoS_2 can be altered when the sample is illuminated with intense laser intensity. As shown in Figure 2a, the pristine CTAB-MoS_2 flake exhibits a weak A_{1g} peak and a strong photoluminescence (PL) signal. After strong laser illumination, the intensity of the A_{1g} peak increases dramatically while the intensity of PL spectra significantly declines. Further multipeak and low-temperature PL analysis reveals that the decrease of PL intensity results from the vanishing of A trion and A biexciton peaks and the weakening of A and B exciton peaks (Figure S5).[23] The change of the Raman spectrum under large laser power may imply a structural change of CTAB-MoS_2. After the strong laser illumination, the thickness of the sample decreases to ~43% of its original value (Figure 2b, from ~30 to ~13 nm), which perfectly coincides with the thickness ratio of d(CTAB-MoS_2)/$d(MoS_2)$. Furthermore, cross-sectional HRTEM image of a laser-treated sample proves that the interlayer distance reduces to 0.67 nm after laser illumination, very close to that of pure MoS_2 (Figure S6). These results indicate that the intercalated CTA^+ cations have been extruded to the surrounding area by the heat induced by laser illumination, leaving pure MoS_2 crystal at the laser-treated area.

To investigate the origin of the abnormal Raman peak of the CTAB-MoS_2 sample, we studied the evolution of its Raman

https://doi.org/10.1021/acs.nanolett.3c01543
Nano Lett. 2023, 23, 5342−5349

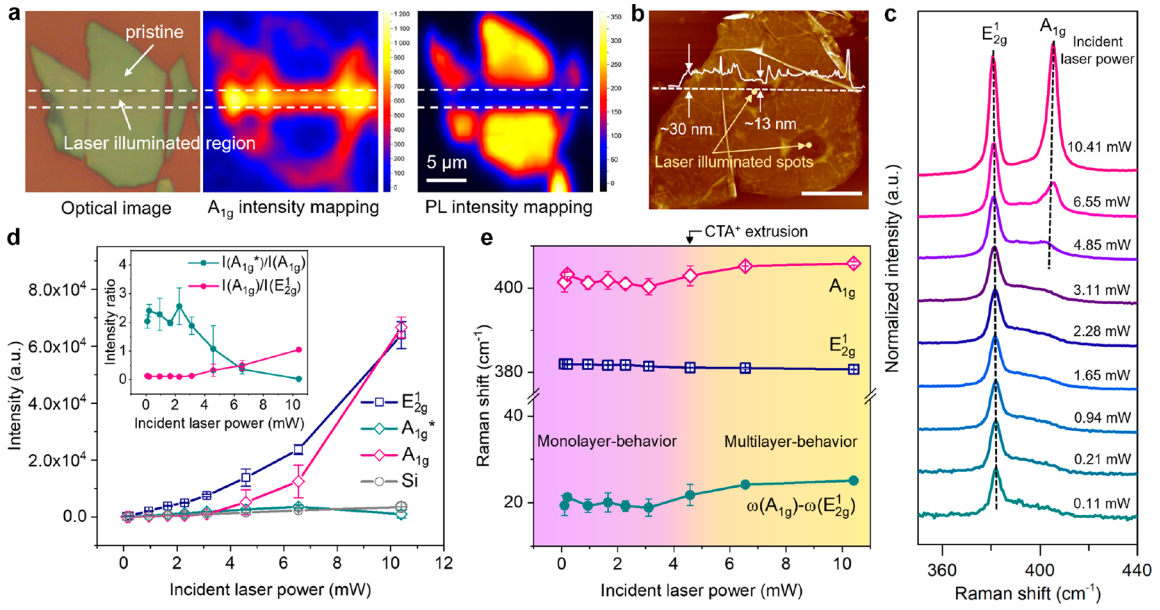

Figure 2. Influence of laser power on Raman spectra. (a) Optical image, A_{1g} intensity mapping and PL intensity mapping of a CTAB-MoS_2 flake treated with strong laser along the dashed lines. (b) Atomic force microscope (AFM) morphology of the CTAB-MoS_2 thin flakes after strong laser treatment. The solid line is the height profile along the dashed line. Scale bar: 5 μm. (c) Evolution of Raman spectra with increasing incident laser power. (d) Evolution of the intensity of E^1_{2g}, A_{1g}*, and A_{1g} peaks with increasing incident laser power. Inset is the evolution of the intensity ratio of $I(A_{1g}^*)/I(A_{1g})$ and $I(A_{1g})/I(E^1_{2g})$. The peak intensity and peak position are extracted from the fitting of Raman spectra. (e) Evolution of the peak position and peak interval of E^1_{2g} and A_{1g} peaks with increasing incident laser power.

spectra under different incident laser powers (Figure 2c). The increase in the incident laser power will enhance the intensities of Raman peaks and will also locally heat the sample through the photothermal effect, as indicated by the red-shift of the E^1_{2g} peak. With increasing the laser power, the peak intensity of the silicon substrate (~520 cm^{-1}) shows a normal linear increase (Figure 2d). However, the intensity of the E^1_{2g} peak of MoS_2 exhibits a nonlinear increase. Along with the rapid increase of the E^1_{2g} peak intensity, the initially negligible A_{1g} peak appears and sharply increases and finally surpasses the intensity of the E^1_{2g} peak when the laser power exceeds 10.41 mW. As a comparison, the intensity of the A_{1g}* peak first undergoes a mild increase under low laser powers (≤6.55 mW) but rapidly disappears when the intensity of the A_{1g} peak sharply increases. The peak interval between E^1_{2g} and A_{1g} modes is ~20 cm^{-1} at a low laser power (≤3.11 mW), which is similar to a monolayer MoS_2. At high laser power (10.41 mW), however, the peak interval reaches 25.1 cm^{-1} (Figure 2e), indicating that the Raman spectrum has already changed to be akin to that in pure multilayer MoS_2.[24−26] The changes in peak intensity and in peak interval are irreversible as the A_{1g} peak still remains its position and relative intensity when the laser power is reset at a lower level. This phenomenon is also observed under a 633 nm wavelength laser (Figure S7). To avoid nonlinear optical effects for Raman signals under high laser powers, we also tracked the evolution of Raman spectrum obtained at a low laser power after the samples were treated under high laser powers, which shows a similar evolution phenomenon (Figure S8).

According to the PL intensity mapping shown in Figure 2a, it is also reasonable to assume that the interlayer coupling of MoS_2 layers in CTAB-MoS_2 is very weak. Thus, the multilayer or even bulk CTAB-MoS_2 behaves like multiple MoS_2 monolayers with strong PL intensity, revealing a direct bandgap behavior.[27] After the strong laser illumination, the PL signal is greatly weakened, and the sample shows optical properties similar to multilayer or bulk MoS_2. This hypothesis is also proved by Kelvin probe force microscopy (KPFM, Figure S9). At the laser illuminated spot, the work function of the sample increases, which is consistent with the previous research that multilayer MoS_2 has a higher work function than monolayers.[28] All of these results suggest that the evolution of the Raman spectrum of CTAB-MoS_2 under laser illumination results from the extrusion of intercalated CTA^+ cations from MoS_2 interlayers. In this extrusion process, the abnormal Raman spectrum gradually becomes a normal one, implying that the abnormal A_{1g}* peak originates from the interaction between the MoS_2 and the CTA^+ intercalation.

The absence of out-of-plane vibrational mode has been hardly observed in other organic-intercalated MoS_2 systems,[21,29−31] and thus it arouses two major questions: (1) what the physical origin of the A_{1g}* peak is and (2) why the A_{1g} peak is strongly suppressed in CTAB-MoS_2. To clarify these questions, we conducted a series of control experiments. At first, we clarify that the A_{1g}* peak does not originate from the lattice vibration of the CTAB or the solvent themselves (Figure S10). Then, we conducted polarized Raman measurements on the *ab* lattice plane of CTAB-MoS_2 samples (Figure 3a),[32,33] where the incident laser is intrinsically polarized along the *y*-axis that can be labeled as (0, 1, 0). After passing through a half-wave plate, the polarized laser is rotated into (cos θ, sin θ, 0). The Raman intensities of A_{1g} and A_{1g}* clearly show anisotropy along different rotation angles (θ) (Figures 3b, S11, and S12), which are well proportional to $\cos^2\theta$ (illustrated by the blue line) and reaches the maximum at θ = 0°. The polarized Raman spectra of the A_{1g} peak correspond well with previous studies,[5,34,35] and the similar behavior of the A_{1g}* peak suggests that it shows the same symmetry as that of the A_{1g} peak. We further conducted low-temperature Raman analysis to study the temperature-dependent behavior of the

https://doi.org/10.1021/acs.nanolett.3c01543
Nano Lett. 2023, 23, 5342−5349

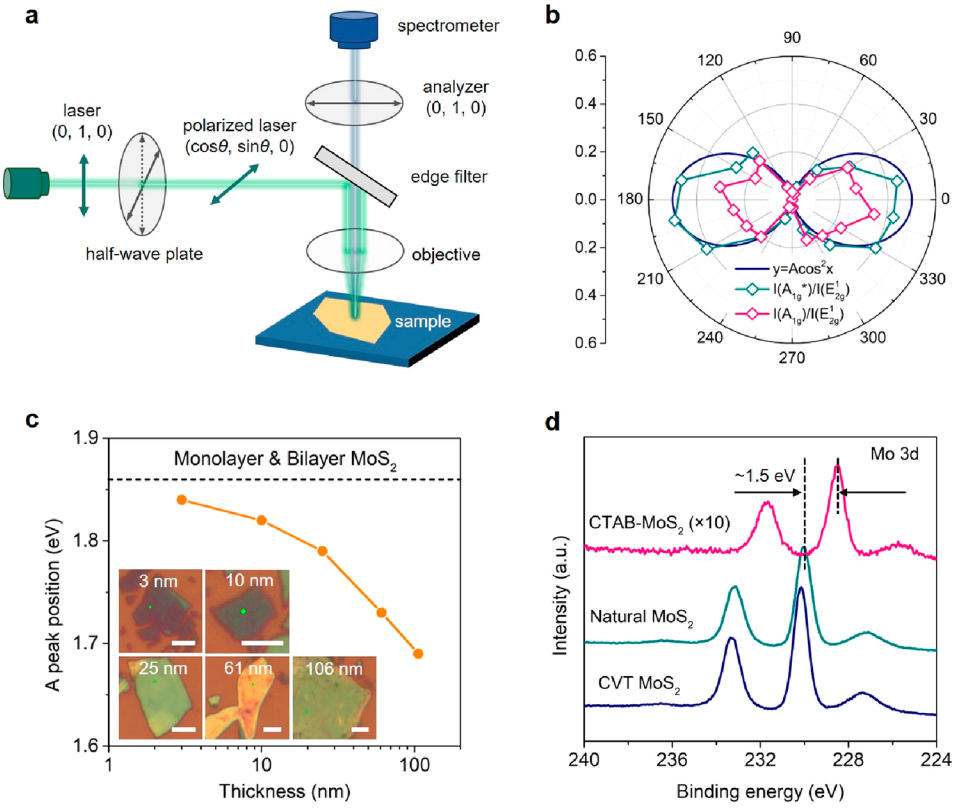

Figure 3. In-depth study of the abnormal Raman signal. (a) Experimental setup of the polarized Raman spectra. (b) Angular dependence of the Raman intensities of A_{1g} and A_{1g}* peaks. The solid blue line shows the relationship following $y = A \cos^2 \theta$. (c) Blue-shift of the A peak position with sample thicknesses. Inset shows the optical images of the samples. Scale bars: 3 μm. (d) XPS spectra of Mo 3d orbitals of bulk CTAB-MoS_2, natural MoS_2, and CVT MoS_2. The CTAB-MoS_2 shifts to a lower binding energy by ~1.5 eV.

Raman peaks. It is known that the Raman peak position of MoS_2 linearly depends on lattice temperature.[36] As shown in Figure S13, the temperature coefficient of the A_{1g}* peak is very close to that of the A_{1g} peak, while the E^1_{2g} peak has a different temperature coefficient. This proves that the A_{1g}* peak results from a similar vibration mode as the A_{1g} peak. Combined with the experimental result on the evolution of the broad A_{1g}* peak into the normal A_{1g} peak (Figure 2c), we can conclude that the A_{1g}* peak should correspond to the subpeak of the red-shifted and suppressed A_{1g} peak, which might be attributed to the interactions between MoS_2 and intercalated CTAB layers. In other words, all the abnormality in Raman spectra can be explained by the fact that the original A_{1g} peak is severely red-shifted and suppressed in CTAB-MoS_2. However, it is still surprising that the A_{1g} peak can be red-shifted by more than 15 cm^{-1}, and its intensity could be much weaker than that of the E^1_{2g} peak, which is not discovered in previous literature.

The reason for this phenomenon is an interesting question. We exclude the transition from direct bandgap in monolayer MoS_2 to indirect bandgap in multilayer MoS_2 from the main reason for the abnormal Raman behavior because the transition of band structures can only slightly change the peak positions of E^1_{2g} or A_{1g} and will not greatly suppress either of them.[37,38] On the other hand, as the A_{1g} mode originates from the out-of-plane vibration of Mo−S bond (see the inset figure of Figure 1d), it could be greatly suppressed when CTA^+ chains restrain the vibration of the Mo−S bond through the possible chemical bonds or vdWs forces.[5,13,14,39] Apart from this hypothesis, we also attribute the abnormal Raman behavior to electron doping (or n-doping) because the A_{1g} mode shows much stronger coupling effect with electrons than the E^1_{2g} mode.[18] To testify this, we conducted thickness-dependent PL measurements of CTAB-MoS_2 flakes and performed X-ray photoelectron spectroscopy (XPS) on bulk CTAB-MoS_2. As shown in Figures S14 and 3c, the PL peak of the thickest CTAB-MoS_2 flake (~106 nm, Figure S14) has red-shifted by ~0.17 eV in comparison with the mechanically exfoliated monolayer MoS_2, which is strong evidence of n-doping of MoS_2 by CTA^+ intercalation.[19] Figure 3d shows the XPS spectra of CTAB-MoS_2, natural MoS_2 (used as the ingredient for electrochemical intercalation), and chemical vapor transport (CVT) synthesized MoS_2. It can be found that natural MoS_2 and CVT MoS_2 have similar XPS signals with the Mo 3d peak deviating by less than 0.1 eV. However, the Mo 3d peak of CTAB-MoS_2 blue-shifts by more than 1.5 eV compared to that of the natural MoS_2, indicating that the n-doping effect has triggered a reduction of Mo^{4+} to Mo^{3+} or even lower valence.[40,41] Following the results reported by Chakraborty et al.,[18] the red-shift of the A_{1g} peak of our CTAB-MoS_2 sample by more than 15 cm^{-1} corresponds to a doping concentration of up to 8×10^{13} cm^{-2} for each layer. The Hall measurement of our bulk CTAB-MoS_2 crystal (50 μm in thickness) yields a carrier concentration of 1.24×10^{20} cm^{-3}, corresponding to 3.55×10^{15} cm^{-2} for each layer, while that of pristine MoS_2 is 1.84×10^{12} cm^{-2} for each layer (Table S1). The CTAB-MoS_2 field-effect transistors (FETs) do not show clear on/off characteristic, also verifying that the CTAB-MoS_2 is heavily n-doped (Figure S15). We believe that the electron concentration extracted based on the Raman analysis is an underestimation because the abnormal A_{1g}* peak may not

https://doi.org/10.1021/acs.nanolett.3c01543
Nano Lett. 2023, 23, 5342−5349

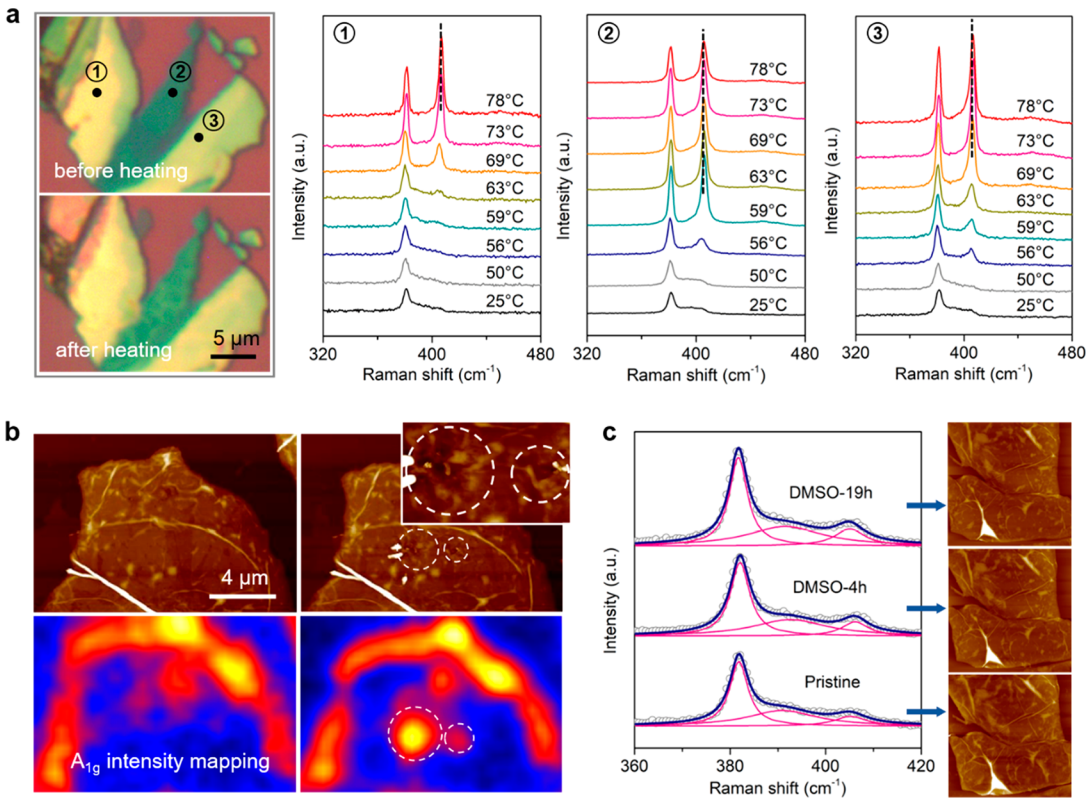

Figure 4. Impact of heating, mechanical pressure, and solvent on Raman spectra. (a) *In situ* heating experiment and the corresponding Raman spectra. The numbers 1, 2, and 3 indicate thick, thin, and moderate thickness flakes, respectively. (b) AFM image and A_{1g} intensity mapping of a CTA^+-MoS_2 thin flake before and after nanoindentation experiment. Dashed circles outline the indented area. (c) Evolution in Raman spectra of pristine CTA^+-MoS_2 thin flake and the same flake after 4 and 19 h DMSO treatment. Shown on the right are the corresponding AFM images, which show minor differences.

follow the relationship in the literature[18] at such a high doping concentration. The actual doping concentration should be more close to the Hall measurement results, which also reaches a high value that can hardly be achieved by other approaches such as surface engineering or electric-field-induced doping.[42−46] Previous work has suggested a semiconductor-to-metal (STM) transition under such strong n-doping,[47] but it is surprising that our CTAB-MoS_2 samples still remain a semiconducting 2H phase, as revealed by the strong E^1_{2g} peak and strong PL intensity (Figure S14) that cannot be obtained in the metallic 1T phase.[48−50]

Following the above analyses, we can try to explain the abnormality in Raman spectra. Because of the strong n-doping and the restrain of the Mo−S bond, the original out-of-plane vibrational mode is greatly suppressed, such that the A_{1g} peak red-shifts toward the E^1_{2g} peak with a severely weakened intensity. Because of the weak interlayer coupling in the intercalated CTAB-MoS_2, the whole spectrum is the sum of Raman signal contributed by each layer. The doping effect may be induced during the electrochemical intercalation process, in which the CTA^+ ions are intercalated into MoS_2 interlayers, forming electric double layers at the CTA^+/MoS_2 interfaces and inducing a massive number of electrons in MoS_2. After the laser treatment, the intercalations are extruded out to the surrounding regions or degraded, so that the electrons are simultaneously released and the out-of-plane vibration of Mo−S (A_{1g} mode) is reformed.

As aforementioned, the removal of intercalations leads to the normalization of the A_{1g} peak. This may imply some ways to convert the intercalated CTAB-MoS_2 sample exhibiting a behavior of highly doped multiple monolayers back to a normal multilayer MoS_2. We first conducted *in situ* global heating experiments on the samples (Figure 4a), where the temperature was calibrated by monitoring the thermal shift of the Raman peak of silicon.[51] As shown in Figure 4a, all the three flakes undergo the abnormality-to-renormalization transition of the A_{1g} peak, but the transition temperature depends on the sample thickness, which is lower for the thinner sample. This result indicates that the departure of the intercalations happens layer by layer, and the thinner samples are less tolerant to high temperature. The *in situ* migration of CTA^+ in a thick CTAB-MoS_2 flake was recorded (Figure S16). The optical contrast in the optical image of the sample changes after the heating process, further revealing the migration of CTA^+. We then applied local mechanical pressure by indenting a CTAB-MoS_2 sample with an AFM tip[52,53] and compared the Raman intensity mapping around the normal A_{1g} peak (395−410 cm^{-1}) before and after the indentation to reveal its structural changes. The indentation process causes a local deformation of the sample (Figure 4b). The originally weak A_{1g} peak becomes significant at the indented spot (inside dashed circle). These results can be well explained by the extrusion of the intercalations induced by the heating in laser treatment or global heating and the mechanical squeezing in nanoindentation. The extrusion of the intercalations eliminates the heavy doping effect and has the out-of-plane vibration of Mo−S (A_{1g} mode) reappear, which is irreversible unless another electrochemical intercalation of CTAB is applied. The

https://doi.org/10.1021/acs.nanolett.3c01543
Nano Lett. 2023, 23, 5342−5349

fact that the interlayer distance has reduced to be very close to that of pure MoS_2 after the laser treatment is a strong evidence of the extrusion of CTA^+ (Figure 2b, inset of Figure 4b, and Figure S6).

Although the CTAB-MoS_2 sample seems to be converted to a nonintercalated, multilayer MoS_2 sample by heating or nanoindentation, it is quite stable upon a solvent immersion at room temperature. After a 19 h immersion in DMSO, the intensity of the A_{1g} peak only shows a very slight increase, indicating that the n-doping level is only slightly reduced (see Figure 4c). However, the morphology of this sample remains almost unchanged, and the suppression of the A_{1g} peak is still obvious. Such a result suggests that the CTA^+ ions can hardly be removed by organic chemicals through the diffusion out of the interlayers, and CTAB-MoS_2 is well resistant to solvent treatment at room temperature.

In conclusion, we synthesized CTAB-intercalated semiconducting MoS_2 superlattices and observed abnormal Raman behavior in their thin flakes. The red-shifted and suppressed A_{1g} peak is attributed to the restraint of the Mo−S out-of-plane vibration and the heavy n-doping effect. The sample remains its direct bandgap even for thick flakes and bulk crystals, and the multilayer flakes exhibit the same Raman and PL behaviors of monolayer MoS_2 due to the weak interlayer coupling. Laser exposure, heating, and mechanical pressure could trigger the diffusion or degradation of the intercalated organic and eliminate the intercalation effect. However, the CTAB-MoS_2 is stable under room temperature and has good resistance to organic solvent. The relatively stable chemical properties and robust electron concentration are major advantages of this intercalated system, which can hardly be achieved by gating the MoS_2 flakes or surface engineering.[54] With remarkable electron concentration and direct bandgap, the CTAB-MoS_2 demonstrates great potential in flexible and nanoscale thermal electric devices.

■ ASSOCIATED CONTENT

Supporting Information

The Supporting Information is available free of charge at https://pubs.acs.org/doi/10.1021/acs.nanolett.3c01543.

Methods; experimental setup of the sample preparation; characterization of the interlayer distance of CTAB-MoS_2; Raman spectra of CTAB-MoS_2 thin flakes; Raman spectra under different laser wavelengths; PL analysis of a partially laser-treated CTAB-MoS_2 sample; characterization of the interlayer distance of laser-treated CTAB-MoS_2; Raman spectra under different laser powers; evolution of Raman spectra after laser treatment; characterization of the weak interlayer coupling; Raman spectra of the intercalated organic; polarized Raman analysis under an excitation wavelength of 532 nm; polarized Raman analysis under an excitation wavelength of 488 nm; temperature-dependent behavior of Raman spectra; PL analysis of CTAB-MoS_2 samples with different thicknesses; electron-doping effect of MoS_2 by CTA^+ intercalation; *in situ* heating experiments on CTAB-MoS_2 (PDF)

■ AUTHOR INFORMATION

Corresponding Authors

Ping-Heng Tan − *State Key Laboratory of Superlattices and Microstructures, Institute of Semiconductors, Chinese Academy of Sciences, Beijing 100083, China;* orcid.org/0000-0001-6575-1516; Email: phtan@semi.ac.cn

Chunlei Wan − *State Key Laboratory of New Ceramics and Fine Processing, School of Materials Science and Engineering, Tsinghua University, Beijing 100084, China;* orcid.org/0000-0002-2032-9060; Email: wancl@mail.tsinghua.edu.cn

Kai Liu − *State Key Laboratory of New Ceramics and Fine Processing, School of Materials Science and Engineering, Tsinghua University, Beijing 100084, China;* orcid.org/0000-0002-0638-5189; Email: liuk@tsinghua.edu.cn

Authors

Yufei Sun − *State Key Laboratory of New Ceramics and Fine Processing, School of Materials Science and Engineering, Tsinghua University, Beijing 100084, China;* Present Address: Aerospace Research Institute of Materials & Processing Technology, Beijing 100076, China

Shujia Yin − *State Key Laboratory of New Ceramics and Fine Processing, School of Materials Science and Engineering, Tsinghua University, Beijing 100084, China*

Ruixuan Peng − *State Key Laboratory of New Ceramics and Fine Processing, School of Materials Science and Engineering, Tsinghua University, Beijing 100084, China*

Jia Liang − *State Key Laboratory of New Ceramics and Fine Processing, School of Materials Science and Engineering, Tsinghua University, Beijing 100084, China;* orcid.org/0000-0002-1765-2852

Xin Cong − *State Key Laboratory of Superlattices and Microstructures, Institute of Semiconductors, Chinese Academy of Sciences, Beijing 100083, China*

Yi Li − *College of Mathematics and Physics, Beijing University of Chemical Technology, Beijing 100029, China*

Chenyu Li − *State Key Laboratory of New Ceramics and Fine Processing, School of Materials Science and Engineering, Tsinghua University, Beijing 100084, China*

Bolun Wang − *State Key Laboratory of New Ceramics and Fine Processing, School of Materials Science and Engineering, Tsinghua University, Beijing 100084, China*

Miao-Ling Lin − *State Key Laboratory of Superlattices and Microstructures, Institute of Semiconductors, Chinese Academy of Sciences, Beijing 100083, China;* orcid.org/0000-0001-5838-8237

Complete contact information is available at: https://pubs.acs.org/10.1021/acs.nanolett.3c01543

Author Contributions

Y.S., S.Y., R.P., and J.L. contributed equally to this work.

Notes

The authors declare no competing financial interest.

■ ACKNOWLEDGMENTS

This work was financially supported by the China Key National R&D Plan (No. 2017YFA0700705), National Key R&D Program of China (2022YFA1203400), Basic Science Center Project of NSFC under Grant 52388201, National Natural Science Foundation of China (51972193, 12004377, and 11874350), CAS Key Research Program of Frontier Sciences (Grants ZDBS-LY-SLH004 and XDPB22), and CAS Project for Young Scientists in Basic Research (YSBR-026). We thank Dr. Yu-Chen Leng for his help and assistance on the Raman measurement.

https://doi.org/10.1021/acs.nanolett.3c01543
Nano Lett. 2023, 23, 5342−5349

■ ABBREVIATIONS

CTAB, cetyltrimethylammonium bromide; TMDC, transition-metal dichalcogenide; AFM, atomic force microscopy; DMSO, dimethyl sulfoxide; NMP, *N*-methylpyrrolidone; ACN, acetonitrile; DMF, dimethylformamide; XRD, X-ray diffraction; HRTEM, high-resolution transmission electron microscopy; vdWs, van der Waals; PL, photoluminescence; KPFM, Kelvin probe force microcopy; XPS, X-ray photoelectron spectroscopy; CVT, chemical vapor transport; FET, field-effect transistor; STM, semiconductor to metal.

■ REFERENCES

(1) Butler, S. Z.; Hollen, S. M.; Cao, L.; Cui, Y.; Gupta, J. A.; Gutierrez, H. R.; Heinz, T. F.; Hong, S. S.; Huang, J.; Ismach, A. F.; Johnston-Halperin, E.; Kuno, M.; Plashnitsa, V. V.; Robinson, R. D.; Ruoff, R. S.; Salahuddin, S.; Shan, J.; Shi, L.; Spencer, M. G.; Terrones, M.; Windl, W.; Goldberger, J. E. Progress, challenges, and opportunities in two-dimensional materials beyond graphene. *ACS Nano* **2013**, *7* (4), 2898−926.

(2) Novoselov, K. S.; Mishchenko, A.; Carvalho, A.; Castro Neto, A. H. 2D materials and van der Waals heterostructures. *Science* **2016**, *353* (6298), aac9439.

(3) Tan, C.; Cao, X.; Wu, X. J.; He, Q.; Yang, J.; Zhang, X.; Chen, J.; Zhao, W.; Han, S.; Nam, G. H.; Sindoro, M.; Zhang, H. Recent Advances in Ultrathin Two-Dimensional Nanomaterials. *Chem. Rev.* **2017**, *117* (9), 6225−6331.

(4) Wu, J.-B.; Wang, H.; Li, X.-L.; Peng, H.; Tan, P.-H. Raman spectroscopic characterization of stacking configuration and interlayer coupling of twisted multilayer graphene grown by chemical vapor deposition. *Carbon* **2016**, *110*, 225−231.

(5) Zhang, X.; Qiao, X. F.; Shi, W.; Wu, J. B.; Jiang, D. S.; Tan, P. H. Phonon and Raman scattering of two-dimensional transition metal dichalcogenides from monolayer, multilayer to bulk material. *Chem. Soc. Rev.* **2015**, *44* (9), 2757−85.

(6) Li, X.-L.; Han, W.-P.; Wu, J.-B.; Qiao, X.-F.; Zhang, J.; Tan, P.-H. Layer-Number Dependent Optical Properties of 2D Materials and Their Application for Thickness Determination. *Adv. Funct. Mater.* **2017**, *27* (19), 1604468.

(7) Cong, X.; Liu, X.-L.; Lin, M.-L.; Tan, P.-H. Application of Raman spectroscopy to probe fundamental properties of two-dimensional materials. *npj 2D Mater. Appl.* **2020**, *4* (1), 13.

(8) Wang, J.; Luo, X.; Li, S.; Verzhbitskiy, I.; Zhao, W.; Wang, S.; Quek, S. Y.; Eda, G. Determination of Crystal Axes in Semimetallic T′-MoTe2by Polarized Raman Spectroscopy. *Adv. Funct. Mater.* **2017**, *27* (14), 1604799.

(9) Wang, G.; Li, X.; Wang, Y.; Zheng, Z.; Dai, Z.; Qi, X.; Liu, L.; Cheng, Z.; Xu, Z.; Tan, P.; Zhang, Z. Interlayer Coupling Behaviors of Boron Doped Multilayer Graphene. *J. Phys. Chem. C* **2017**, *121* (46), 26034−26043.

(10) Liu, B.; Abbas, A.; Zhou, C. Two-Dimensional Semiconductors: From Materials Preparation to Electronic Applications. *Adv. Electron. Mater.* **2017**, *3* (7), 1700045.

(11) Wang, B.; Sun, Y.; Ding, H.; Zhao, X.; Zhang, L.; Bai, J.; Liu, K. Bioelectronics-Related 2D Materials Beyond Graphene: Fundamentals, Properties, and Applications. *Adv. Funct. Mater.* **2020**, *30* (46), 2003732.

(12) Wang, X.; Wang, B.; Zhang, Q.; Sun, Y.; Wang, E.; Luo, H.; Wu, Y.; Gu, L.; Li, H.; Liu, K. Grain-Boundary Engineering of Monolayer MoS2 for Energy-Efficient Lateral Synaptic Devices. *Adv. Mater.* **2021**, *33* (32), No. e2102435.

(13) Lee, C.; Yan, H.; Brus, L. E.; Heinz, T. F.; Hone, J.; Ryu, S. Anomalous lattice vibrations of single- and few-layer MoS2. *ACS Nano* **2010**, *4* (5), 2695−700.

(14) Zhang, X.; Han, W. P.; Wu, J. B.; Milana, S.; Lu, Y.; Li, Q. Q.; Ferrari, A. C.; Tan, P. H. Raman spectroscopy of shear and layer breathing modes in multilayer MoS2. *Phys. Rev. B* **2013**, *87* (11), 115413.

(15) Sun, Y.; Wang, Y.; Wang, E.; Wang, B.; Zhao, H.; Zeng, Y.; Zhang, Q.; Wu, Y.; Gu, L.; Li, X.; Liu, K. Determining the interlayer shearing in twisted bilayer MoS2 by nanoindentation. *Nat. Commun.* **2022**, *13* (1), 3898.

(16) Conley, H. J.; Wang, B.; Ziegler, J. I.; Haglund, R. F., Jr.; Pantelides, S. T.; Bolotin, K. I. Bandgap engineering of strained monolayer and bilayer MoS2. *Nano Lett.* **2013**, *13* (8), 3626−30.

(17) Liu, K.; Zhang, L.; Cao, T.; Jin, C.; Qiu, D.; Zhou, Q.; Zettl, A.; Yang, P.; Louie, S. G.; Wang, F. Evolution of interlayer coupling in twisted molybdenum disulfide bilayers. *Nat. Commun.* **2014**, *5*, 4966.

(18) Chakraborty, B.; Bera, A.; Muthu, D. V. S.; Bhowmick, S.; Waghmare, U. V.; Sood, A. K. Symmetry-dependent phonon renormalization in monolayer MoS2transistor. *Phys. Rev. B* **2012**, *85* (16), 161403.

(19) Mao, N.; Chen, Y.; Liu, D.; Zhang, J.; Xie, L. Solvatochromic effect on the photoluminescence of MoS(2) monolayers. *Small* **2013**, *9* (8), 1312−5.

(20) Wan, C.; Gu, X.; Dang, F.; Itoh, T.; Wang, Y.; Sasaki, H.; Kondo, M.; Koga, K.; Yabuki, K.; Snyder, G. J.; Yang, R.; Koumoto, K. Flexible n-type thermoelectric materials by organic intercalation of layered transition metal dichalcogenide TiS2. *Nat. Mater.* **2015**, *14* (6), 622−7.

(21) He, Q.; Lin, Z.; Ding, M.; Yin, A.; Halim, U.; Wang, C.; Liu, Y.; Cheng, H. C.; Huang, Y.; Duan, X. In Situ Probing Molecular Intercalation in Two-Dimensional Layered Semiconductors. *Nano Lett.* **2019**, *19* (10), 6819−6826.

(22) Ding, H.; Wang, Y.; Liang, Y.; Qin, F. Preparation and Characterization of Cetyl Trimethylammonium Intercalated Sericite. *Advances in Materials Science and Engineering* **2014**, *2014* (2014), 1−8.

(23) Pandey, J.; Soni, A. Unraveling biexciton and excitonic excited states from defect bound states in monolayer MoS2. *Appl. Surf. Sci.* **2019**, *463*, 52−57.

(24) Luo, X.; Zhao, Y.; Zhang, J.; Xiong, Q.; Quek, S. Y. Anomalous frequency trends in MoS2 thin films attributed to surface effects. *Phys. Rev. B* **2013**, *88* (7), 075320.

(25) Li, S.-L.; Miyazaki, H.; Song, H.; Kuramochi, H.; Nakaharai, S.; Tsukagoshi, K. Quantitative Raman Spectrum and Reliable Thickness Identification for Atomic Layers on Insulating Substrates. *ACS Nano* **2012**, *6* (8), 7381−7388.

(26) Lu, X.; Luo, X.; Zhang, J.; Quek, S. Y.; Xiong, Q. Lattice vibrations and Raman scattering in two-dimensional layered materials beyond graphene. *Nano Res.* **2016**, *9* (12), 3559−3597.

(27) Eda, G.; Yamaguchi, H.; Voiry, D.; Fujita, T.; Chen, M.; Chhowalla, M. Photoluminescence from chemically exfoliated MoS2. *Nano Lett.* **2011**, *11* (12), 5111−6.

(28) Choi, S.; Shaolin, Z.; Yang, W. Layer-number-dependent work function of MoS2 nanoflakes. *J. Korean Phys. Soc.* **2014**, *64* (10), 1550−1555.

(29) Jiang, Y.; Wang, J.; Zhang, D.; Luo, Y.; Yang, T.; Gong, J.; Zhang, F.; Zhang, X.; Tong, Z. CTAB-assisted synthesis of dissilient hollow spherical MoS2 for efficient hydrogen evolution. *Materials Research Express* **2019**, *6* (3), 035001.

(30) Chhetri, S.; Adak, N.; Samanta, P.; Murmu, N.; Kuila, T. Exploration of Mechanical and Thermal Properties of CTAB-Modified MoS2/LLDPE Composites Prepared by Melt Mixing. *Journal of Composites Science* **2018**, *2* (3), 37.

(31) Lin, Z.; Liu, Y.; Halim, U.; Ding, M.; Liu, Y.; Wang, Y.; Jia, C.; Chen, P.; Duan, X.; Wang, C.; Song, F.; Li, M.; Wan, C.; Huang, Y.; Duan, X. Solution-processable 2D semiconductors for high-performance large-area electronics. *Nature* **2018**, *562* (7726), 254−258.

(32) Liu, X.-L.; Zhang, X.; Lin, M.-L.; Tan, P.-H. Different angle-resolved polarization configurations of Raman spectroscopy: A case on the basal and edge plane of two-dimensional materials. *Chinese Physics B* **2017**, *26* (6), 067802.

(33) Rawat, D.; Singh, A.; Singh, N. K.; Soni, A. Anisotropic light-matter interactions in the single-crystal topological insulator bismuth selenide. *Phys. Rev. B* **2023**, *107* (15), 155203.

https://doi.org/10.1021/acs.nanolett.3c01543
Nano Lett. 2023, 23, 5342−5349

(34) Wang, Y.; Cong, C.; Qiu, C.; Yu, T. Raman spectroscopy study of lattice vibration and crystallographic orientation of monolayer MoS2 under uniaxial strain. *Small* **2013**, *9* (17), 2857−61.
(35) Zhao, Y.; Luo, X.; Li, H.; Zhang, J.; Araujo, P. T.; Gan, C. K.; Wu, J.; Zhang, H.; Quek, S. Y.; Dresselhaus, M. S.; Xiong, Q. Interlayer breathing and shear modes in few-trilayer MoS2 and WSe2. *Nano Lett.* **2013**, *13* (3), 1007−1015.
(36) Yan, R.; Simpson, J. R.; Bertolazzi, S.; Brivio, J.; Watson, M.; Wu, X.; Kis, A.; Luo, T.; Hight Walker, A. R.; Xing, H. G. Thermal conductivity of monolayer molybdenum disulfide obtained from temperature-dependent Raman spectroscopy. *ACS Nano* **2014**, *8* (1), 986−993.
(37) Li, T.; Guo, W.; Ma, L.; Li, W.; Yu, Z.; Han, Z.; Gao, S.; Liu, L.; Fan, D.; Wang, Z.; Yang, Y.; Lin, W.; Luo, Z.; Chen, X.; Dai, N.; Tu, X.; Pan, D.; Yao, Y.; Wang, P.; Nie, Y.; Wang, J.; Shi, Y.; Wang, X. Epitaxial growth of wafer-scale molybdenum disulfide semiconductor single crystals on sapphire. *Nat. Nanotechnol.* **2021**, *16* (11), 1201−1207.
(38) Yoon, H. H.; Fernandez, H. A.; Nigmatulin, F.; Cai, W.; Yang, Z.; Cui, H.; Ahmed, F.; Cui, X.; Uddin, M. G.; Minot, E. D.; Lipsanen, H.; Kim, K.; Hakonen, P.; Hasan, T.; Sun, Z. Miniaturized spectrometers with a tunable van der Waals junction. *Science* **2022**, *378* (6617), 296−299.
(39) Chhetri, S.; Adak, N. C.; Samanta, P.; Mandal, N.; Kuila, T.; Murmu, N. C. Investigation of mechanical and thermal properties of the cetyltrimethylammonium bromide functionalized molybdenum disulfide (MoS2)/epoxy composites. *Polym. Bull.* **2018**, *75* (1), 327−343.
(40) Yang, H.; Chen, X.; Hu, G.; Chen, W.-T.; Bradley, S. J.; Zhang, W.; Verma, G.; Nann, T.; Jiang, D.-e.; Kruger, P. E.; Wang, X.; Tian, H.; Waterhouse, G. I. N.; Telfer, S. G.; Ma, S. Highly efficient electrocatalytic hydrogen evolution promoted by O−Mo−C interfaces of ultrafine β-Mo2C nanostructures. *Chemical Science* **2020**, *11* (13), 3523−3530.
(41) Dizayee, W.; Ying, M.; Griffin, J.; Alqahtani, M. S.; Buckley, A.; Fox, A. M.; Gehring, G. A. Investigation of the distribution of localised and extended states in amorphous MoOx. *AIP Adv.* **2018**, *8* (5), 055118.
(42) Lu, X.; Utama, M. I. B.; Wang, X.; Xu, W.; Zhao, W.; Owen, M. H. S.; Xiong, Q. Gate-Tunable Resonant Raman Spectroscopy of Bilayer MoS2. *Small* **2017**, *13* (35), 1701039.
(43) Kiriya, D.; Tosun, M.; Zhao, P.; Kang, J. S.; Javey, A. Air-stable surface charge transfer doping of MoS(2) by benzyl viologen. *J. Am. Chem. Soc.* **2014**, *136* (22), 7853−6.
(44) Lin, J. D.; Han, C.; Wang, F.; Wang, R.; Xiang, D.; Qin, S.; Zhang, X. A.; Wang, L.; Zhang, H.; Wee, A. T.; Chen, W. Electron-doping-enhanced trion formation in monolayer molybdenum disulfide functionalized with cesium carbonate. *ACS Nano* **2014**, *8* (5), 5323−9.
(45) Yang, L.; Majumdar, K.; Liu, H.; Du, Y.; Wu, H.; Hatzistergos, M.; Hung, P. Y.; Tieckelmann, R.; Tsai, W.; Hobbs, C.; Ye, P. D. Chloride molecular doping technique on 2D materials: WS2 and MoS2. *Nano Lett.* **2014**, *14* (11), 6275−80.
(46) Park, H. Y.; Lim, M. H.; Jeon, J.; Yoo, G.; Kang, D. H.; Jang, S. K.; Jeon, M. H.; Lee, Y.; Cho, J. H.; Yeom, G. Y.; Jung, W. S.; Lee, J.; Park, S.; Lee, S.; Park, J. H. Wide-range controllable n-doping of molybdenum disulfide (MoS2) through thermal and optical activation. *ACS Nano* **2015**, *9* (3), 2368−76.
(47) Voiry, D.; Mohite, A.; Chhowalla, M. Phase engineering of transition metal dichalcogenides. *Chem. Soc. Rev.* **2015**, *44* (9), 2702−12.
(48) Fang, Y.; Pan, J.; He, J.; Luo, R.; Wang, D.; Che, X.; Bu, K.; Zhao, W.; Liu, P.; Mu, G.; Zhang, H.; Lin, T.; Huang, F. Structure Re-determination and Superconductivity Observation of Bulk 1T MoS2. *Angew. Chem., Int. Ed. Engl.* **2018**, *57* (5), 1232−1235.
(49) Liu, L.; Wu, J.; Wu, L.; Ye, M.; Liu, X.; Wang, Q.; Hou, S.; Lu, P.; Sun, L.; Zheng, J.; Xing, L.; Gu, L.; Jiang, X.; Xie, L.; Jiao, L. Phase-selective synthesis of 1T' MoS2 monolayers and heterophase bilayers. *Nat. Mater.* **2018**, *17* (12), 1108−1114.
(50) Tan, S. J. R.; Sarkar, S.; Zhao, X.; Luo, X.; Luo, Y. Z.; Poh, S. M.; Abdelwahab, I.; Zhou, W.; Venkatesan, T.; Chen, W.; Quek, S. Y.; Loh, K. P. Temperature- and Phase-Dependent Phonon Renormalization in 1T'-MoS2. *ACS Nano* **2018**, *12* (5), 5051−5058.
(51) Tsu, R.; Hernandez, J. G. Temperature dependence of silicon Raman lines. *Appl. Phys. Lett.* **1982**, *41* (11), 1016−1018.
(52) Lee, C.; Wei, X.; Kysar, J. W.; Hone, J. Measurement of the elastic properties and intrinsic strength of monolayer graphene. *Science* **2008**, *321* (5887), 385−8.
(53) Sun, Y.; Pan, J.; Zhang, Z.; Zhang, K.; Liang, J.; Wang, W.; Yuan, Z.; Hao, Y.; Wang, B.; Wang, J.; Wu, Y.; Zheng, J.; Jiao, L.; Zhou, S.; Liu, K.; Cheng, C.; Duan, W.; Xu, Y.; Yan, Q.; Liu, K. Elastic Properties and Fracture Behaviors of Biaxially Deformed, Polymorphic MoTe2. *Nano Lett.* **2019**, *19* (2), 761−769.
(54) Li, Y.; Xu, C. Y.; Hu, P.; Zhen, L. Carrier control of MoS2 nanoflakes by functional self-assembled monolayers. *ACS Nano* **2013**, *7* (9), 7795−804.

https://doi.org/10.1021/acs.nanolett.3c01543
Nano Lett. 2023, 23, 5342−5349